Polymer Testing 100 (2021) 107262

Contents lists available at ScienceDirect

Polymer Testing

journal homepage: www.elsevier.com/locate/polytest

Structural integrity of adhesively bonded 3D-printed joints

Mohammad Reza Khosravani [a,*], Payam Soltani [b], Kerstin Weinberg [c], Tamara Reinicke [a]

[a] Chair of Product Development, University of Siegen, Paul-Bonatz-Str. 9-11, 57068 Siegen, Germany
[b] Centre of Engineering, Faculty of Computing, Engineering and the Built Environment, Birmingham City University, Birmingham, B4 7XG, UK
[c] Chair of Solid Mechanics, University of Siegen, Paul-Bonatz-Str. 9-11, 57068 Siegen, Germany

ARTICLE INFO

Keywords:
Additive manufacturing
Single-lap joint
Fracture
Adhesive joint

ABSTRACT

Fabrication of polymeric components with complex geometry has been increased in the recent years. As additive manufacturing (AM) showed its unique capabilities, it has been widely used in production of geometrically-complex parts. Although various types of bonding have been developed, utilizing adhesive joints is common in different polymeric structures. In the current study, influence of 3D printing parameters and adhesive thickness on the performance of adhesively bonded joints have been studied. To this aim, we have used fused deposition modeling (FDM) process and polylactic acid (PLA) material to fabricate single-lap joints. The specimens are fabricated under different printing conditions to determine influence of printing parameters on the mechanical behavior of the joints. Moreover, adhesive with three different thicknesses was used to investigate effect of adhesive thickness on the structural integrity of the 3D-printed joints. Additionally, a series of finite element analysis was performed and agreement between experimental observation and numerical results has been documented. As FDM process has garnered significant attention, the outcomes of this study can be used for further development.

1. Introduction

Additive manufacturing (AM), commonly known as three-dimensional (3D) printing presents unique capabilities compared to traditional manufacturing processes. This rapid manufacturing technique, is being utilized in different applications, such as aerospace, electronics, dentistry, and healthcare monitoring [1–4]. According to ASTM 2792-12a [5], AM has been classified into seven methods. AM uses a 3D model data to build up a component in layers by depositing material. Although AM initially used for fabrication of prototypes, this manufacturing process has been currently used for the direct fabrication of functional end-use products. Here, we used an extrusion-based AM method to fabricate adhesively bonded joints.

Based on the significant growth of AM in recent years, various engineering issues such sustainability aspects [6], environmental impact [7], and structural integrity [8] have been investigated in this field. Considering different applications of 3D-printed components, fatigue and fracture studies of these parts attracted a lot of research interest in the last few years [9–13] and very recently fracture behavior of additively manufactured components was fully reviewed in [14]. This rapid growth of interest in AM applications from a large range of industrial sectors has led to the urgent need for design and fabrication of 3D printed components with bigger dimensions, lighter weight and with a more complex topology. To respond to this need and to overcome the size limit of commercial 3D printers, it is required that the component gets divided and printed into its sub-components with simple shape and geometry first, and then the whole structure gets assembled using a typical joining method like adhesive bonding. In previous studies, adhesively-bonded components have a lighter weight with fewer critical stress concentration points in their bonding area, and adhesive bonding method is a highly preferable joining method in comparison to other similar techniques like bolted joints or welding [15,16]. Adhesive bonding is a well-known, widely studied technique and also a typical method for binding different types of materials [17–23]. Adhesive joints with different adherends have been also studied in details from different mechanical prospectives such as stress analysis [22], bonding strength [20], fracture [24], and fatigue degradation [25]. However, to the best of our knowledge, there are still limited numbers of research available focusing on the mechanical design and characteristics of adhesive joints with 3D-printed polymeric adherends. Experimental investigations on mechanical characterization of single-lap adhesive joints (SLAJs) with 3D-printed adherends are performed in [26]. Fused deposition modeling (FDM) is employed to print the adherends using a green Polyacticacid (PLA) thermoplastic filament. Epoxy adhesive is used to bond the adherends and the PLA components are printed in two printing directions (flatwise and edgewise). Two

* Corresponding author.
E-mail address: mohammadreza.khosravani@uni-siegen.de (M.R. Khosravani).

https://doi.org/10.1016/j.polymertesting.2021.107262
Received 2 February 2021; Received in revised form 18 May 2021; Accepted 30 May 2021
Available online 5 June 2021

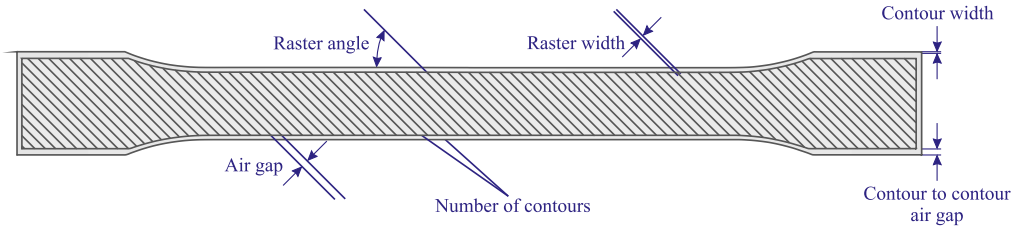

Fig. 1. A schematic of specimens based on ASTM D638 and FDM printing parameters.

different bonding configurations are also considered (with a wave shape interlocking mechanism and without the interlocking mechanism). The experimental results reveal that the printing direction of the adherends and also modifying the morphology of the PLA surfaces in the bonding region have a strong effect on the load capacity and strength of the joint, while the importance of the surface preparation is much bigger. Mechanical strength of the SLAJs with 3D-printed ABS sheets, manufactured by FDM technique, is investigated in [27]. A zig-zag configuration is considered for the boding area of adherends to increase the contact area and provide interlocking mechanism. Two different types of adhesive and different printing parameters for adherends are considered. The experimental results show that, with a proper design of bonding area, adhesively bonded structures with 3D-printed adherends could enhance the strength of the structure similar to a single component with the base material.

Due to limited numbers of research in the area of mechanical performance and failure of adhesive joints with 3D-printed adherends, in this research, we aimed at providing a holistic study on adhesively bonded 3D-printed structures considering the impacts of printing parameters of the adherends (such as raster angle, raster width, and layer thickness). The study also tends to find the optimum thickness of the adhesive layer in which the adhesive joint presents the maximum mechanical strength. A set of experimental tests supported by a 3D-FEM are used to create required data toward these contributions. To do so, in this paper, it is focused on the strength and fracture of SLAJs made up of the 3D-printed PLA sheets (very popular type of filaments used in commercial 3D printers). A common epoxy adhesive is used, and the adherends are printed with different printing parameters (i.e., different raster angles, raster widths, and layer thicknesses) and also at different adhesive thicknesses. All these experiments are also supported by a numerical finite element model (FEM) that covers all conditions, and help to provide a generalized parametric model of the SLAJs with 3D-printed adherends. To this end, this paper is organized as follows: in Section 2, specimen preparation and configurations of the SLAJs are described in details. Section 3 explains the experimental tests and FE numerical simulations of 3D-printed SLAJs. Section 4 presents a discussion and finally, a conclusion has been furnished in Section 5.

2. Specimen preparation

In the current study, PLA material was utilized to print test coupons based on the FDM method. Considering effects and impacts of printing parameters on the mechanical behavior of 3D-printed parts, we have fabricated and examined dog-bone shaped specimens to determine basic mechanical properties and document effects of printing parameters. In this context, dog-bone shaped samples were made considering the following three different printing parameters:

- Raster direction: 0°, 45°, and 90°.
- Raster width: 0.75 mm and 1 mm.
- Layer thickness: 0.2 mm and 0.5 mm.

Raster direction is defined as printing direction relative to the loading direction. Raster width refers to the width of the deposition path [28]. The third considered parameter is layer thickness which is the layer height of each printed layer [29]. It is noteworthy that the 3D model of the dog-bone shaped specimens are designed according to the ASTM D638 [30]. In Fig. 1, FDM printing parameters in a dog-bone shaped specimen are schematically illustrated. In this study, to cover all combinations of the aforementioned printing parameters, twelve dog-bone parts are needed, and considering three specimens for each case (to check the repeatability) a set of total 36 dog-bone shaped specimens are fabricated and tested.

Table 1
Printing parameters and properties of PLA and 3D-printed specimens.

Printing parameters	Values	PLA parameters	Values
Raster angle (°)	±45	Density (gr/cm^3)	1.21
Raster width (mm)	0.75, 1	Melting point (°C)	~160
Number of contours	2	Glass transition (°C)	~65
Infill percentage (%)	100	Elongation at yield (%)	2
Layer thickness (mm)	0.2, 0.5	Elongation at break (%)	6
Bed temperature (°C)	55	Filament diameter (mm)	1.75
Nozzle diameter (mm)	0.8	Diameter tolerance (mm)	±0.05
Printing speed (mm/s)	30	Moisture absorption (ppm)	1968
Nozzle temperature (°C)	215	Izod impact strength (J/m)	16

In order to determine the strength of adhesively bonded single-lap joint, test coupons are prepared based on ASTM D3163-01 [31]. In detail, two parts of each specimens were designed in a CAD platform, saved as "stl." format, printed using FDM process, and later bonded. PLA properties and printing parameters are summarized in Table 1. Although raster width and layer thickness were changed in fabrication of different specimens, all other printing parameters were kept constant for all specimens.

In design of specimens, two contours were considered and infill density was set to 100%. In order to ensure printing quality of the test coupons, visual appearance of printed parts were investigated and failed parts were replaced. In Fig. 2 a 3D-printed single-lap joint and its geometries are shown.

In the present study, after printing components of the single-lap joints, they are bonded via an epoxy adhesive [32] to finish fabrication of test coupons. More in deep, an appropriate fixture was designed and manufactured to maintain the alignment of the two parts of single-lap joints during curing period and also to make the thickness of the adhesive layer precisely adjustable. Fig. 3 shows exploded view of the fabricated fixture. In order to speed up the manufacturing process of the joints, we have made five fixtures.

According to ASTM D3163-01, SLAJs are made with overlap region about one-quarter of the specimen length. It should be noted that the additional step was added at the end of each part in order to avoid rotational moments when the specimens are clamped on the tensile machine.

Selection of adhesive is important issue in fabrication of adhesively bonded joints. Indeed, type of adhesive and its properties has a significant effect on the bond strength. In this study, all specimens for destructive testing were bonded with an industrial grade epoxy adhesive with extended work life. In detail, we used two components adhesive LOCTITE® EA 9466™ from Henkel (Düsseldorf, Germany) which is an industrial grade epoxy adhesive. According to the technical datasheet of manufacturer, it was necessary to keep assembled parts from moving during cure. The adhesive cured at room temperature for 24 hours according to the manufacturer's datasheet. The main

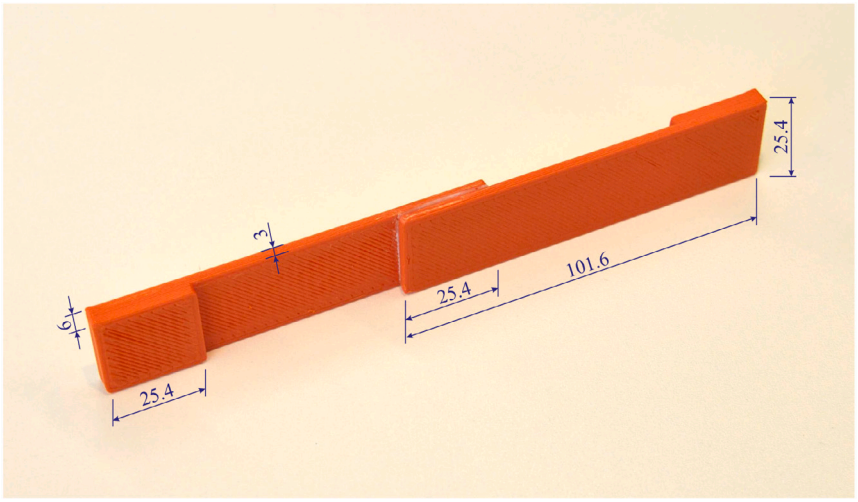

Fig. 2. A 3D-printed single-lap joint (Dimensions in mm).

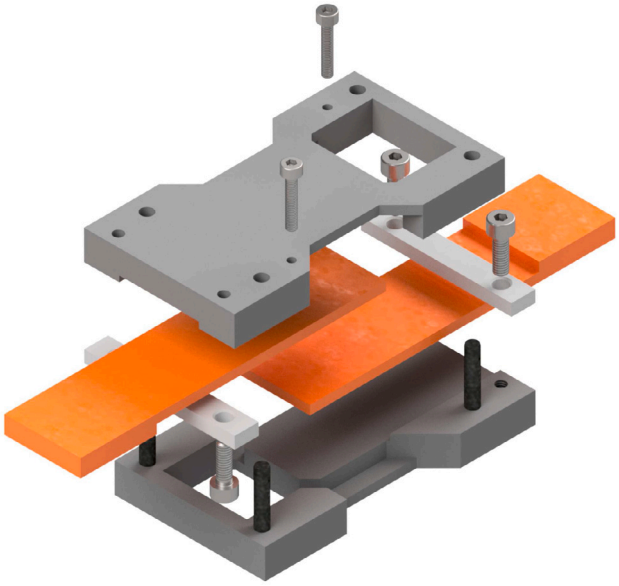

Fig. 3. Exploded view of the fabricated fixture used to ensure alignment of adherents in manufacturing of the specimens.

properties of the utilized adhesive are reported in Table 2. All printed parts were cleaned, washed, and subsequently dried prior using the adhesive.

In the present study, SLAJs with different adhesive layer thicknesses (a) 0.2 mm, (b) 0.3 mm, and (c) 0.4 mm were fabricated to investigate effects of the adhesive thickness on the fracture of the joints. All specimens were kept at room temperature for 24 h after filling the gap of the overlap area in the fixture with the adhesive. In the following section, details of experimental tensile tests on dog-bone shaped specimens and SLAJs are explained.

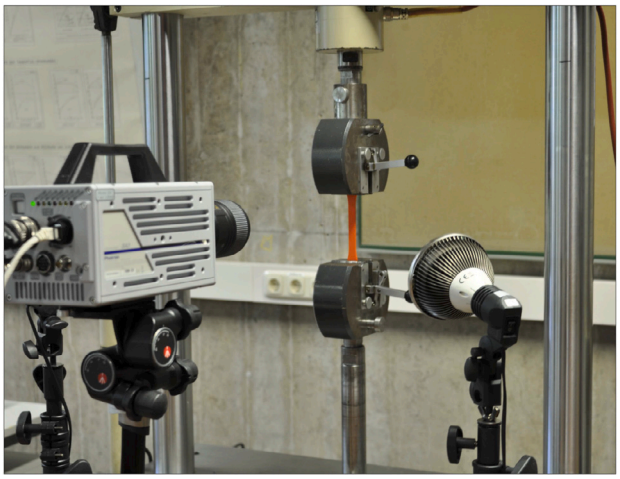

Fig. 4. A 3D-printed dog-bone shaped specimens under tensile test conditions.

3. Mechanical fracture in 3D-printed joints

3.1. Experimental tests

According to ASTM D638, a series of tests was performed on the dog-bone shaped specimens with a constant cross-head speed of 5 mm/min. Based on the obtained results, effects of printing parameters on elastic modulus of examined parts are determined. Fig. 4 shows a PLA printed dog-bone shaped specimen under tensile test conditions. For all examined specimens, the load versus displacement was recorded. The obtained curves of these tensile tests conformed that almost all specimens showed a linear load–displacement behavior that is followed by a drop at failure (see Fig. 8).

Standard tensile tests are also performed on 3D-printed adhesively bonded joints a hydraulic tensile test machine equipped with a 15 kN load cell. The machine has cross-head speed range of 0.01 mm/s to 30 mm/s. In order to avoid the likely effect of the displacement rate, a

Table 2
Mechanical properties of the used adhesive.

Shear strength (MPa)	Tensile strength (MPa)	Tensile modulus (MPa)	Impact strength (J/m^2)	T_g (°C)
37	32	1718	5.8	62

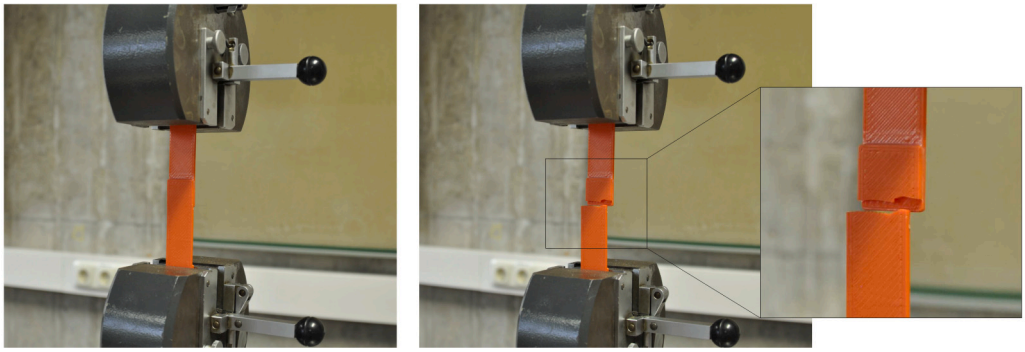

Fig. 5. 3D-printed adhesively bonded joint, before (left), and after (right) tensile test.

series of the tests was performed under displacement control condition with a constant rate of 1 mm/min for all single-lap joint specimens. All the tests were performed under room conditions with temperature and relative humidity of 23 ± 3 °C and 50 ± 5%, respectively. In Fig. 5 a 3D-printed adhesively bonded joint before and after the tensile test is illustrated. In this study, 36 adhesively bonded specimens were examined and test results showed repeatable results.

An overload in adhesively bonded joints leads to failure in different modes. Four different failure modes of adhesive joints are schematically illustrated in Fig. 6. Specimen geometry, quality of the bond, loading, and relative strength between adhesive and material determined type of failure mode. The main failure modes in a SLAJ are: (a) adhesive failure, (b) cohesive failure, (c) failure in adjacent structure, and (d) yielding of adherents. When the bondline is weakened, an adhesive failure is more likely to occur. It means that shear strength of adhesive is weaker than the material strength. It can be result of an environmental impact or caused by incorrect manufacturing process. In cohesive failure, as the most common type of failure mode, crack initiates in the adhesive and propagates till final fracture occurs. When the shear strength of the utilized adhesive is larger than the strength of material, fracture appeared just adjacent to the adhesion region and the third type of failure mode is occurred. The last failure mode is the result of overload in a bonded joint, caused by the low strength adherents.

Based on the single-lap joint test, as one of the most common tests which presents structural behavior of adhesive joints, in the present study three types of failure modes were observed. In detail, a few specimens showed first and third types of failures (adhesive failure and failure in adjacent structure) while cohesive failure was most of the occurred failure mode in the examined specimens. These failure modes in fractured specimens are shown in Fig. 7.

As stated above, 36 different SLAJs were tested and three different failure modes were observed: (1) adhesive failure, (2) cohesive failure, and (3) failure in adjacent structure. The dominant failure mode observed among all samples was the cohesive failure. In detail, cohesive failure occurred in 25 specimens along with seven specimens with adhesive failure and other four with failure in adjacent structure. This is a clear indication of well-performed experiment and demonstrates that test coupons were fabricated properly. An average load–displacement curves of specimens with three different failure modes are shown in Fig. 8 (left). Since each failure mode has occurred in several specimens, here average of fracture load is illustrated for each failure mode. For instance, cohesive failure occurred in 25 specimens, and 1986.2 is an average of all fracture loads in the specimens with this failure mode. Moreover, the overall linear stiffness of the SLAJ in mode (1) is lower than the other two modes (it is about 680.2 N/m) while the maximum linear stiffness belongs to the SLAJs in mode 2 (about 995.7 N/m). Adhesive failure mode in interfacial bond failure shows low bonding strength and poor bonding capability and adhesive failure mode shows the lowest fracture load (1123.5 ± 15.1 N). Fig. 8 (right) represents the corresponding nominal stress–strain curves of specimens at each failure mode. Taking into account gradual loading of the SLAJ, (i) initial loading with elastic deformation, (ii) a minor softening, (iii) deformation, and (iv) final rupture can be considered as distinct stages in the experimental investigation. Comparison of the curves for different failure modes would be helpful for understanding the strength and stiffness of the 3D-printed joints.

In the cohesive failure mode, maximum fracture load was equal to 1986.2 N. Cohesive failure is considered as a 'good' adhesive bond, because it indicates suitable adhesive curing conditions and good cohesive strength [33]. In fact, in cohesive failure within the adhesive, the maximum strength of the bonded structure has been reached. In several industrial applications cohesive failure is desired mode of failure which indicates the proper selection and application of the adhesive for the given substrate. As in this failure, the damage occurs in the adhesive layer, usually a shorter repair time at a reasonable price is possible.

The obtained results indicated in the cohesive failure mode, the maximum fracture load belongs to the specimens printed with 0.2 mm layer thickness, and raster width of 0.75 mm, which was connected by 0.2 mm adhesive layer. This finding is in agreement with previous studies which showed that in the SLAJs the higher fracture load belongs to thinner adhesive layer [34–36]. For example, in [35] experiments showed that the strength increases as the thickness of the adhesive is reduced. In [37] it was discussed that fracture load of the joint and its strength increases as the thickness of the adhesive decreases. Here, we defined effective stress which is ratio of the measured fracture load to the bonded area. The calculated effective stresses are presented in Table 3. It is noteworthy that, according to the experimental results, specimens with cohesive failure showed higher elastic modulus values than other examined specimens. As it is illustrated in Fig. 8, the slope of the stress–strain curve of the cohesive failure mode is more than other presented failure modes.

Comparison of the experimental findings confirmed that the adhesive thickness of 0.2 mm is an optimum value for the examined 3D-printed parts with respect to the strength of the bonded joint. This experimental result is in excellent agreement with previous studies [38–40]. In [38], based on experimental investigations on the joints with different adhesive thicknesses it was discussed that peak adhesive shear stresses occurred at the interface and increase of the adhesive thickness leads to increase the shear stresses. Later, in [39] test of the single lap joints with different adhesive thicknesses (0.2 to 1.2 mm) showed that joint strength decreases with increase in adhesive thickness. As thicker bondlines have more voids and microcracks, there is a greater probability for earlier failure. Our experimental results are compared and verified with numerical simulation in the following subsection.

3.2. Numerical simulations

In parallel to the experimental tests conducted in this research, a 3D-FEM model of the SLAJ is also developed in ABAQUS® to reveal a better understanding of stress distributions, strength, and failure modes

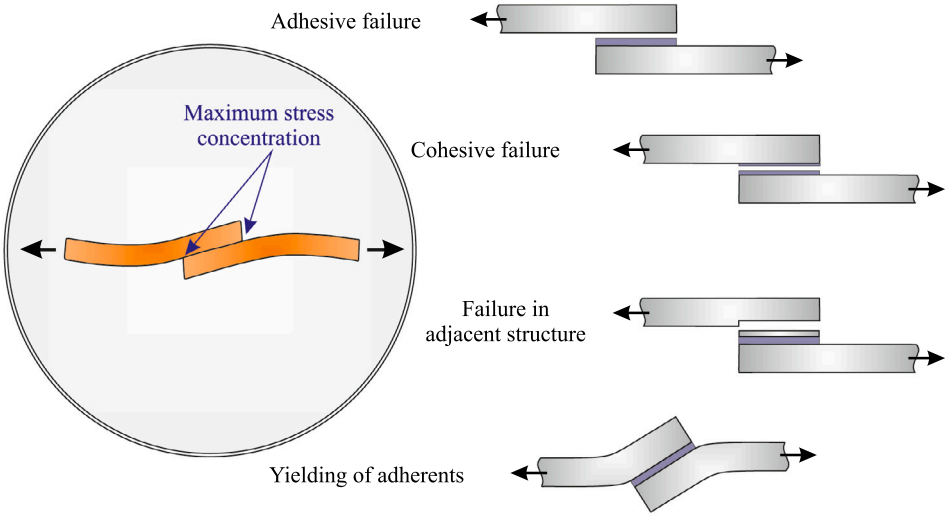

Fig. 6. Schematics of different failure modes in adhesively bonded joints.

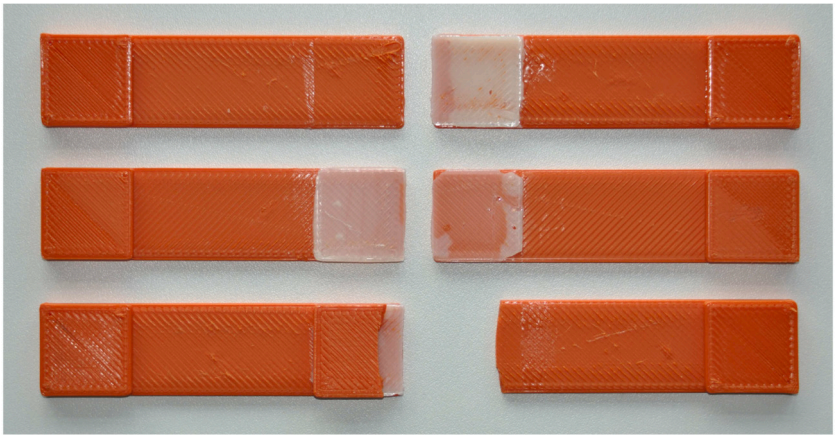

Fig. 7. 3D-printed joints with different failure modes: adhesive failure (top), cohesive failure (middle), and failure in adjacent structure (bottom).

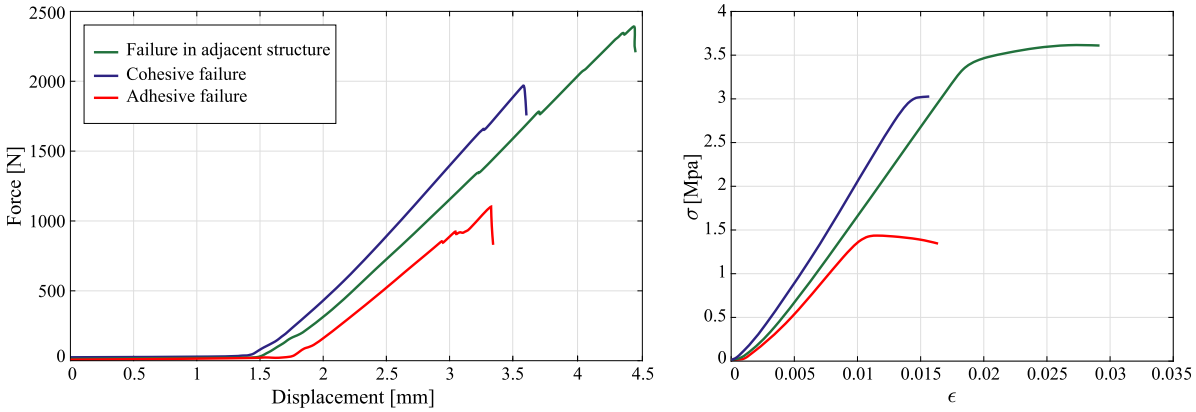

Fig. 8. Force–displacement curves (left), and stress–strain curves (right) of examined specimens with different failure modes.

Table 3
Experimental results considering occurred failure modes.

Failure mode	Fracture load (N)	Maximum displacement (mm)	Effective stress (MPa)
Cohesive failure	1986.2 ± 12.4	2.2 ± 0.6	3.07
Adhesive failure	1123.5 ± 15.1	1.8 ± 0.7	1.74
Failure in adjacent structure	2418.4 ± 10.7	3.1 ± 0.5	3.74

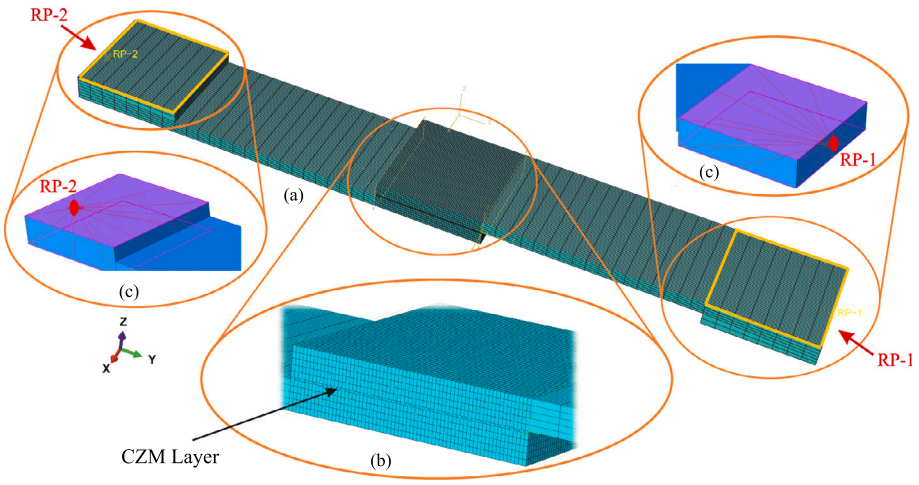

Fig. 9. (a) FE model of the SLAJ, (b) CZM of the adhesive layer, and (c) MPC constraints at the both ends of the model.

of SLAJ with printed PLA adherends. In comparison to 2D FE models, 3D FE modeling of the adhesive joints considers the out-of-plane deformations and also the influences of free surfaces of the structure, leads to more accurate though more complex numerical replica of SLAJs [41]. The developed FE model of SLAJ mimics the topology, loading scenarios and boundary conditions of the printed substrates and tensile test condition of the SLAJ described in the previous section. As the PLA printed dog-bone shapes specimen represent a linear behavior on a wide range of their stress–strain curves under the standard tensile test (according to Fig. 8), it is rational that the corresponding printed adherent substrates are considered as the linear elastic material in the current FE model. An 8-node linear hexagonal (hex) element with reduced integration, considering hourglass control $C3D8R$ is chosen to mesh both the top and the bottom printed adherends. Cohesive zone modeling (CZM) layer is employed to simulate the behavior of the epoxy adhesive. CZM enables the FE model to consider the initiation and evolution of the damage in the adhesive layer and supports multi-modal fracture too. The CZM have been widely used in numerical modeling of adhesive joints and has shown a successful outcomes in simulating the strength, fractures and delamination of these type of structures [42–46]. The cohesive element in ABAQUS employs traction–separation constitutive relations and is commonly used in FE modeling of adhesively bonded joints. In the current FE model, the adhesive is modeled as a single layer of 8-node cohesive hex elements $COH3D8$. Three different adhesive thicknesses of 0.2, 0.3 and 0.4 are considered to cover all different samples used in the experiments. Sweep meshing technique is used with the sweep path along the thickness of the adhesive layer. Tie constraint is precisely defined between the nodes of the top surface of the adhesive layer and its adjacent area on the upper adherend. Similarly,the nodes on the lower surface of the adhesive are tied to its adjacent surface of the lower part. Multi-point kinematic constraint (MPC) is employed to couple all degrees of freedom of nodes located on the top and the bottom surface of the step-shaped section of the substrates to a unique reference point at each end of the SLAJ, as shown in Fig. 9-c (two reference points RP1 and RP2 at two ends of the SLAJ). The MPC constraint helps to simulate the boundary conditions of the SLAJ under axial tensile test similar to the experiment shown in 6. At RP1 all degrees of freedom (DoFs) are encastered, to simulated the fixed conditions at one end and at RP2, the only allowed motion is along the axis of the SLAJ (i.e. y axis or $U2$). On RP2, a gradually increasing displacement is also applied in y direction to demonstrate the elongation of the SLAJ under the experimental tensile test. The resultant force at RP1, as the total reaction force, is considered as an output of the model and the force–displacement curve of the SLAJ is extracted by the FE model.

In Fig. 10 the force–displacement curve of the SLAJ for three different adhesive thickness of 0.2, 0.3, and 0.4 mm are plotted. The adherends of this sample is assumed to be printed with the raster angle of 0°, the raster width of 0.75 mm and the layer thickness of 0.2 mm. The FE results are also compared with experimental load curve of the corresponding SLAJ. All FE models along with the experimental data represent a very flat behavior at very low displacement that is related to the pure elastic shear deformations of the adhesive layer (when displacement is lower than 1 mm). This region is followed by a quasi-linear region in the force–displacement curves that is presenting the load carrying behavior of the adhesive lead to higher reaction forces as the displacement increases. The adhesive failure occurs as this graphs hit their maximum load values (F_{max}). This maximum reaction force demonstrates the load carrying capacity of the joint and is an important parameter in designing the SLAJs. It is clear from this figure that FE models are following the experimental trend and also are predicting the stiffness of the joint (i.e. the slope of the linear part of the curves) and F_{max} with a good agreement with the experiment. It is worth to highlight that the load carrying capacity of the SLAJ predicted by the FE models (for this printed sample) is about $F_{max} = 1818$ N at 4.23 mm elongation while the experiment shows $F_{max} = 1858$ N at 4.02 mm elongation. It is also important to note that aligned with the experiments, the FE model also suggests that the optimum thickness of the adhesive layer is 0.2 mm, as it presents a slightly higher load carrying capacity (F_{max}) in comparison to the other thicknesses presented in Fig. 10. This is in agreement with the higher load carrying capacity of the SLAJ with thickness of 0.2 mm, as described before.

Von Mises stress distribution of the SLAJ is plotted in Figs. 11 for two different adhesive thickness (0.2 and 0.4 mm). The figures demonstrate stress states of the printed adherends just before cohesive failure. These graphs also reveal that the maximum stress level at the SLAJ with adhesive thickness of 0.4 mm is about 14% higher than the one with adhesive thickness of 0.2 mm.

Stress distribution in the adhesive layer plays a crucial role on maintaining the overall stiffness and integrity of the SLAJ structure, so it is vital to have a clear understanding about how stresses are varying across the length of the adhesive bond. Two important stress components are being considered in design of adhesive joints: Peel stress, that is along the thickness of the adhesive layer (S_{33} component at the current model) and also transverse shear component (S_{23} component). The dominant load transfer mode of the SLAJ, under tensile test, occurs under shear mode and distribution of the shear stress in the adhesive layer governs the load carrying task of the joint. However, as the shear deformations increases in the adhesive layer, the substrates also start to bend and this bending lead to the normal peel stress across the adhesive

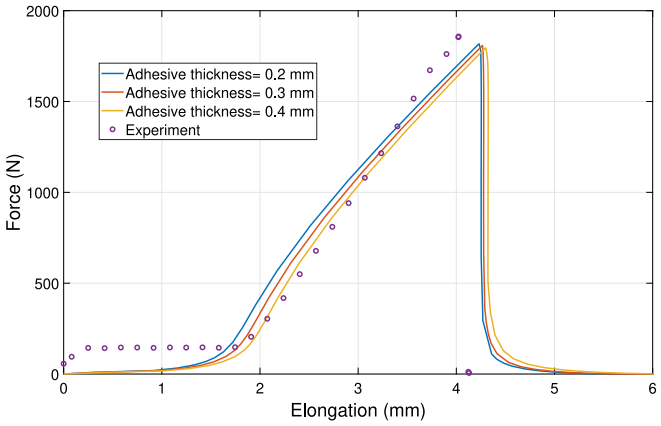

Fig. 10. Force–displacement behavior of the SLAJ under axial tensile load with different adhesive thicknesses-FE results.

thickness. Hence, monitoring the variation of both the peel and shear stress in the adhesive layer is important. Figs. 12-a, b demonstrate the peel stress distributions in the adhesive layer of the model for two different adhesive thicknesses 0.2 and 0.4 mm, correspondingly just before the initiation of the cohesive failure. Uniform and symmetric stress distributions are observed and as expected the same stress patterns are seen for both cases. However, the maximum peel stress at the edges of the overlap region at thickness of 0.4 mm is 4% higher than the one with thickness of 0.2 mm. Shear stress distributions of the adhesive layer with thickness of 0.2 mm and 0.4 mm before the cohesive failure are depicted in Figs. 12-c, d, accordingly. Smooth and symmetric stress distributions are also observed for shear stress but a comparison between the stress level at these figures shows that the maximum shear stress at both adhesive thickness are very close (with differences no more than 0.2%).

To investigate the stress variations across the overlap length of the adhesive, a path is defined at the middle of the cohesive width parallel to the overlap direction (y axis). Variations of the peel stress (S_{33}) and the shear stress (S_{23}) are plotted across this path in Figs. 13. The distance from the edges is normalized by the overlap length (i.e., 25.4 mm as stated in Fig. 2) and the stresses are also normalized based on the maximum average shear stress at each specific thickness (i.e., $\tau_{ave} = \frac{F_{max}}{A}$ where F_{max} is the maximum force at cohesive failure, obtained from Fig. 10, and $A = 25.4 \times 25.4$ mm^2 is the overlap area under shear. The highest level of both peel and shear stress are observed at the vicinity of the vertical edges of the overlap area (at 6% of the normalized distance from both edges). The shear stress goes up to 5.5 τ_{ave} while the peel stress is limited to around 3.2 τ_{ave}. It is also

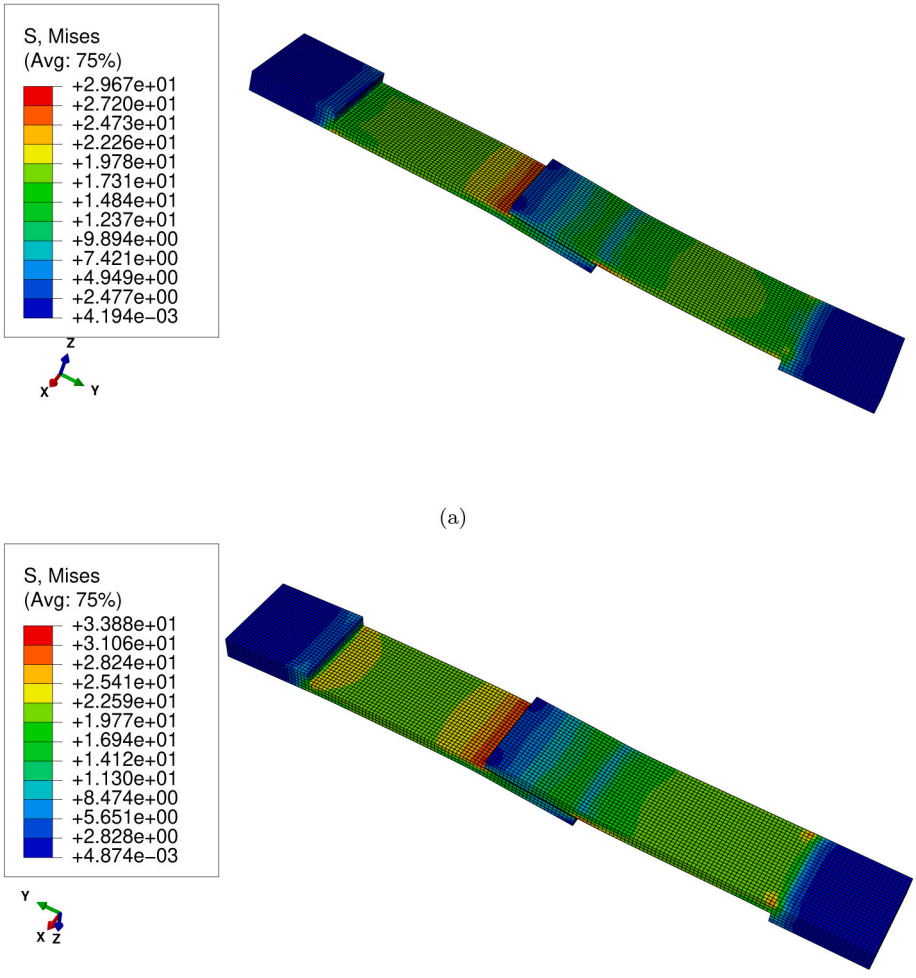

Fig. 11. Von Mises stress distributions of the SLAJ at the cohesive failure point with adhesive thickness of (a) 0.2 mm and (b) 0.4 mm.

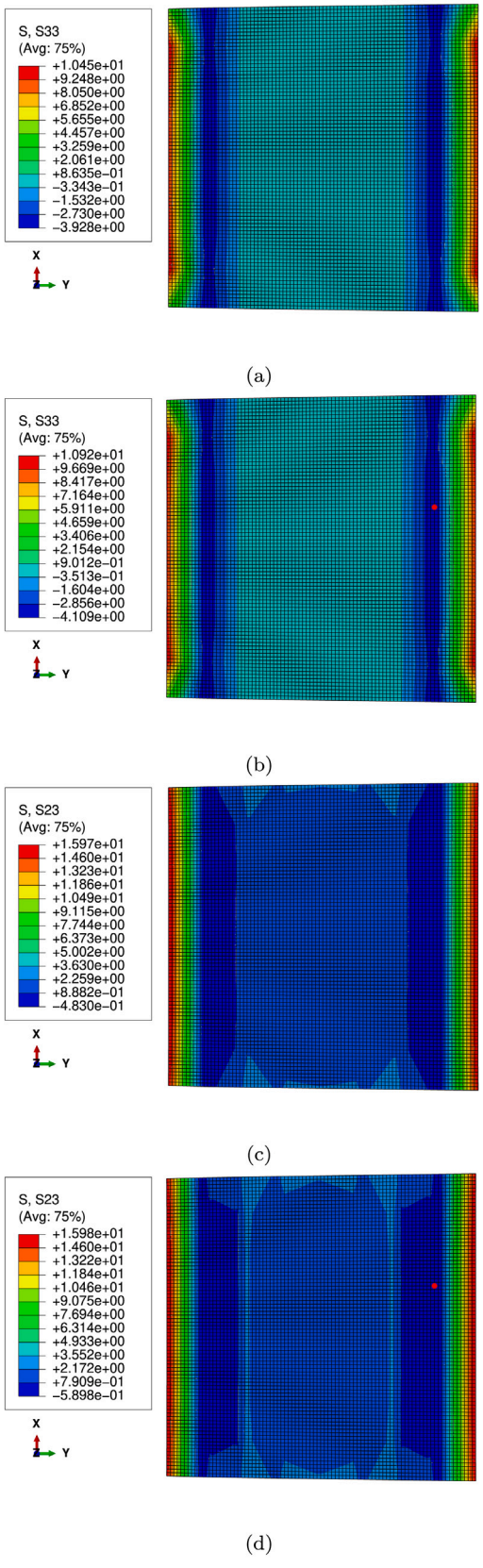

Fig. 12. Stress distribution of adhesive layer: Peel stress with (a) 0.2 mm and (b) 0.4 mm adhesive thickness; Shear stress with (c) 0.2 mm and (d) 0.4 mm adhesive thickness.

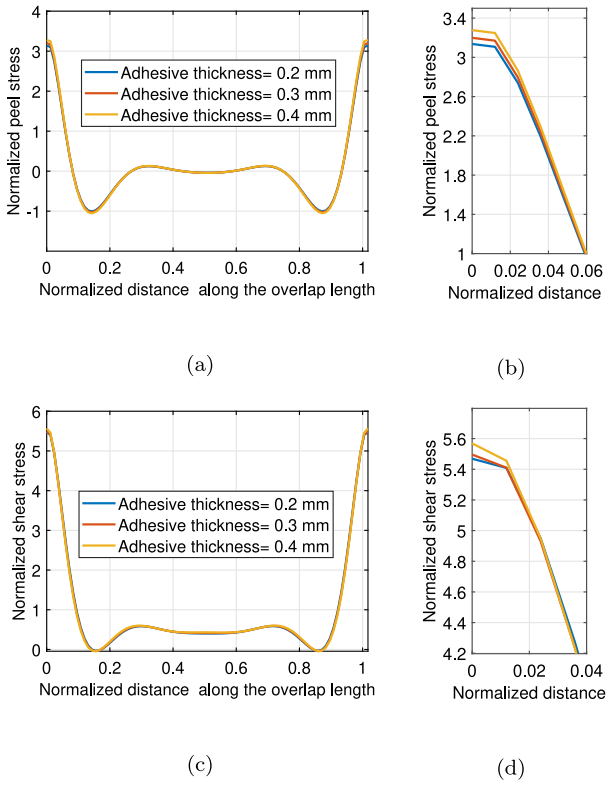

Fig. 13. Stress distribution across the overlap length of the adhesive layer with different thicknesses: (a) Normalized peel stress distributions against the normalized overlap length and (b) its zoom-in view at the edges of the bonding area; (c) Normalized shear stress distribution against the normalized overlap length and (d) its zoom-in view at the edges of the bonding area.

clear from these figure that variations of the peel and shear stress along the overlap path are negligible respect to the thickness of the adhesive (within the range of ± 0.1 mm variations of the adhesive thickness, however at the edges, both peel and shear stress components of the SLAJ with thickness of 0.4 mm is slightly higher than the other two models although the difference is not that much.

4. Discussion

The experimental results showed that cohesive failure was occurred in most of the examined joints (25 out 36 specimens). Also, specimens with cohesive failure indicated higher elastic modulus compared to the specimens with other failure modes. Moreover, it was found that adhesive thickness of 0.2 mm is an optimum thickness for tested PLA single-lap joints. Parallel to the experimental practices, a three dimensional finite element analysis has been performed. In detail, an 8-node linear hex element was used to mesh adherends and CZM was utilized for simulation of epoxy adhesive. The results of simulations confirmed that load carrying capacity of specimens with adhesive thickness of 0.2 mm was slightly higher than thickness of 0.4 mm (approximately around 1%) which shows an good agreement with experimental findings. Since shear and peel stresses play crucial roles in adhesive layer, their distribution in the adhesive layer was considered in the model. According to the numerical results, maximum peel stress in the model with adhesive thickness of 0.4 mm was higher than the one with thickness of 0.2 mm. Therefore, the role of adhesive thickness obtained from numerical model, is affirmed by experimental findings. Since damage and fracture in adhesively bonded joints would require costly and time-consuming repairs or replacement, the presented results provide data which is beneficial for design optimization of the 3D-printed joints and can be used in future computational models.

Our experimental findings indicated that thinner adhesive layer (0.2 mm) has higher mechanical performance compared to thicker adhesive layer (0.3 and 0.4 mm). This result is in agreement with previous research works [47–50]. For instance, in [47] experimental test showed a significant drop in strength of the joints as adhesive thickness increased. It was documented that examination of sections did not show any physical reason for this issue, but numerical simulation of stress state confirmed larger stress concentration factor in thicker adhesive layer. Later, in [50] the same issue was discussed. Specifically, adhesive with different thicknesses was used in SLAJs and results showed that an increase of adhesive layer thickness leads to a decrease in lap-shear strength. In literature several theories have been proposed to explain why the strength of SLAJs decreases as the adhesive thickness increases. Considering occurring failure to the adhesive-adherend interface, a failure criterion based on the interface stresses can explain the thin adhesive layers are stronger than thick layers. Moreover, decrease of strength with increase of adhesive layer thickness might be related to the plastic spreading of the adhesive along the overlap which occurs more rapidly when the adhesive thickness increases.

5. Conclusion

This study investigates mechanical performance, structural integrity and failure behaviors of SLAJs with 3D-printed PLA adherends. The main contributions of this research are concluded and summarized as follows:

- Using the standard tensile test, the cohesive failure mode is observed as the dominant failure mode on SLAJs, regardless of the printing parameters of the PLA adherends and the adhesive thickness.
- Cohesive failure modes are also observed in specimens with high elastic modulus of the PLA adherends.
- Among different adhesive thicknesses used in the experiments, it is shown that the adhesive thickness of 0.2 mm is considered as the optimum adhesive thickness leading to higher mechanical performance and strength against tension compared to the other two values.
- A data-informed three dimensional FE model of the SLAJ was also created to clarify the mechanical performance of the SLAJs observed in the experiments. The material characteristics of the 3D-printed adherends with different printing parameters have been fed into the FE model using a separate set of data obtained from tensile tests on 3D-printed PLA standard dog-bones.
- Outcomes of the FE model support the experimental results and confirms the optimum adhesive thickness, the failure modes and mechanical performances of the SLAJs under axial tension.
- The FEM model also reveals the stress distributions in the bonding area of SLAJs with 3D-printed adherends, and can be used for design optimization of the 3D-printed adhesive joints.

CRediT authorship contribution statement

Mohammad Reza Khosravani: Conceptualization, Methodology, Investigation, Project administration, Writing - Original Draft. **Payam Soltani:** Methodology, Formal analysis, Validation, Writing - Review & Editing. **Kerstin Weinberg:** Writing - Review & Editing. **Tamara Reinicke:** Resources, Funding acquisition, Writing - Review & Editing.

Declaration of competing interest

The authors declare that they have no known competing financial interests or personal relationships that could have appeared to influence the work reported in this paper.

Acknowledgment

This work as part of the project “Smart Production Design Center” (SmaP) is funded by the European Regional Development Fund (ERDF) under the program OP EFRE NRW 2014–2020 (EFRE-0200545).

EUROPÄISCHE UNION
Investition in unsere Zukunft
Europäischer Fonds
für regionale Entwicklung

EFRE.NRW
Investitionen in Wachstum
und Beschäftigung

References

[1] K.V.P. Reddy, I.M. Mirzana, A.K. Reddy, Application of additive manufacturing technology to an aerospace component for better trade-off's, Mater. Today: Proc. 5 (2018) 3895–3902.
[2] M.R. Khosravani, T. Reinicke, 3D-printed sensors: Current progress and future challenges, Sensors Actuators A 305 (2020) 111916.
[3] P. Vasamsetty, T. Pss, D. Kukkala, M. Singamshetty, S. Gajula, 3D printing in dentistry - Exploring the new horizons, Mater. Today: Proc. 26 (2020) 838–841.
[4] S. Nasiri, M.R. Khosravani, Progress and challenges in fabrication of wearable sensors for health monitoring, Sensors Actuators A 312 (2020) 112105.
[5] ASTM F2792 -12 Standard Terminology for Additive Manufacturing Technologies, Standard, American Society for Testing Materials, West Conshohocken, USA, 2012.
[6] M. Mahadevan, A. Francis, A. Thomas, A simulation-based investigation of sustainability aspects of 3D printed structures, J. Build. Eng. 33 (2020) 101735.
[7] M.R. Khosravani, T. Reinicke, On the environmental impacts of 3D printing technology, Appl. Mater. Today 20 (2020) 100689.
[8] Z. Chen, J. Xu, B. Liu, Y. Zhang, J. Wu, Structural integrity analysis of transmission structure inflapping-wing micro aerial vehicle via 3D printing, Eng. Fail. Anal. 96 (2019) 18–30.
[9] T. Liu, X. Tian, M. Zhang, D. Abliz, D. Li, G. Ziegmann, Interfacial performance and fracture patterns of 3D printed continuous carbon fiber with sizing reinforced PA6 composites, Composites A 114 (2018) 368–376.
[10] V. Shanmugam, D.J. Johnson, K. Babu, S. Rajendran, A. Veersasimman, U. Marimuthu, S. Singh, O. Das, R.E. Neisiany, M.S. Hedenqvist, F. Berto, S. Ramakrishna, The mechanical testing and performance analysis of polymer-fibre composites prepared through the additive manufacturing, Polym. Test. 93 (2021) 106925.
[11] M.R. Khosravani, A. Zolfagharian, Fracture and load-carrying capacity of 3D-printed cracked components, Extreme Mech. Lett. 20 (2020) 100692.
[12] G. Qian, Z. Jian, X. Pan, F. Berto, In-situ investigation of fatigue behaviors of Ti-6Al-4V manufactured by selective laser melting, Int. J. Fatigue 133 (2020) 105424.
[13] V. Shanmugam, O. Das, K. Babu, U. Marimuthu, A. Veersasimman, D.J. Johnson, R.E. Neisiany, M.S. Hedenqvist, S. Ramakrishna, F. Berto, Fatigue behaviour of FDM-3D printed polymers, polymeric composites and architected cellular materials, Int. J. Fatigue 143 (2021) 106007.
[14] M.R. Khosravani, F. Berto, M.R. Ayatollahi, T. Reinicke, Fracture behavior of additively manufactured components: A review, Theor. Appl. Fract. Mech. 109 (2020) 102763.
[15] G. Jeevi, S.K. Nayak, M. Abdul Kader, Review on adhesive joints and their application in hybrid composite structures, J. Adhes. Sci. Technol. 33 (2019) 1497–1520.
[16] K.M. Bak, K. Kalaichelvan, G.K. Vijayaraghavan, M. Dinesh, V. Arumugam, Study on the effect of adhesive thickness of single lap joints using acoustic emission and FEA, Insight, Non-Destr. Test. Cond. Monit. 55 (2013) 35–41.
[17] F.L. Matthews, P.F. Kilty, E.W. Godwin, A review of the strength of joints in fibre-reinforced plastics. Part 2. Adhesively bonded joints, Composites 13 (1) (1982) 29–37.
[18] J. Custódio, J. Broughton, H. Cruz, A review of factors influencing the durability of structural bonded timber joints, Int. J. Adhes. Adhes. 29 (2) (2009) 173–185.
[19] M. Yekani Fard, B. Raji, J. Woodward, A. Chattopadhyay, Characterization of interlaminar fracture modes I, II, and I-II of carbon/epoxy composites including in-service related bonding quality conditions, Polym. Test. 77 (2019) 105894.
[20] X. Shang, E.A.S. Marques, J.J.M. Machado, R.J.C. Carbas, D. Jiang, L.F.M. da Silva, Review on techniques to improve the strength of adhesive joints with composite adherends, Composites B 177 (2019) 107363.
[21] P. Molitor, V. Barron, T. Young, Surface treatment of titanium for adhesive bonding to polymer composites: A review, Int. J. Adhes. Adhes. 21 (2) (2001) 129–136.
[22] L.D.C. Ramalho, R.D.S.G. Campilho, J. Belinha, L.F.M. da Silva, Static strength prediction of adhesive joints: A review, Int. J. Adhes. Adhes. 96 (2020) 102451.
[23] L. Guo, J. Liu, H. Xia, X. Li, X. Zhang, H. Yang, Effects of surface treatment and adhesive thickness on the shear strength of precision bonded joints, Polym. Test. 94 (2021) 107063.
[24] S. Budhe, M.D. Banea, S. De Barros, L.F.M. Da Silva, An updated review of adhesively bonded joints in composite materials, Int. J. Adhes. Adhes. 72 (2017) 30–42.

[25] M.M. Abdel Wahab, Fatigue in adhesively bonded joints: A review, Int. Sch. Res. Not. 2012 (2012).
[26] D.K.K. Cavalcanti, M.D. Banea, H.F.M. Queiroz, Mechanical characterization of bonded joints made of additive manufactured adherends, Ann. "Dunarea de Jos" Univ. Galati. Fasc. XII Weld. Equip. Technol. 30 (2019) 27–33.
[27] A. Spaggiari, F. Denti, Mechanical strength of adhesively bonded joints using polymeric additive manufacturing, Proc. Inst. Mech. Eng. C (2019) 0954406219850221.
[28] S.H. Ahn, M. Montero, D. Odell, S. Roundy, P.K. Wright, Anisotropic material properties of fused deposition modelling ABS, Rapid Prototyp. J. 8 (2002) 248–257.
[29] M.R. Khosravani, T. Reinicke, Effects of raster layup and printing speed on strength of 3D-printed structural components, Procedia Struct. Integr. 28 (2020) 720–725.
[30] ASTM D638 -14 Standard Test Method for Tensile Properties of Plastics, Standard, American Society for Testing Materials, West Conshohocken, USA, 2014.
[31] ASTM D3163 -01 Determining Strength of Adhesively Bonded Rigid Plastic Lap-Shear Joints in Shear By Tension Loading, Standard, American Society for Testing Materials, West Conshohocken, USA, 2001.
[32] LOCTITE EA 9466, Henkel Adhesive Technologies, 2020, www.henkel-adhesives.com/de/en/product/structural-adhesives/loctite_ea_9466.html. (Accessed 12 November 2020).
[33] M.R. Khosravani, K. Weinberg, Experimental investigations of the environmental effects on stability and integrity of composite sandwich T-joints, Mater.wiss. Werkst.tech. 48 (2017) 753–759.
[34] L.F.M. da Silva, R.J.C. Carbas, G.W. Critchlow, M.A.V. Figueiredo, K. Brown, Effect of material, geometry, surface treatment and environment on the shearstrength of single lap joints, Int. J. Adhes. Adhes. 29 (2009) 621–632.
[35] J.M. Arenas, J.J. Narbón, C. Alía, Optimum adhesive thickness in structural adhesives joints using statistical techniques based on Weibull distribution, Int. J. Adhes. Adhes. 30 (2010) 160–165.
[36] M. Rośkowicz, J. Godzimirski, A. Komorek, M. Jasztal, The effect of adhesive layer thickness on joint static strength, Materials 14 (2021) 1–14.
[37] A. Adnan, C.T. Sun, Effect of adhesive thickness on joint strength: A molecular dynamics perspective, J. Adhes. 84 (2008) 401–420.
[38] D.M. Gleich, M.J.L. Van Tooren, A. Beukers, Analysis and evaluation of bondline thickness effects on failure load in adhesively bonded structures, J. Adhes. Sci. Technol. 15 (2001) 1091–1101.
[39] L.F.M. da Silva, T.N.S.S. Rodrigues, M.A.V. Figueiredo, M.F.S.D. de Moura, J.A.G. Chousal, Effect of adhesive type and thickness on the lap shear strength, J. Adhes. 82 (2006) 1091–1115.
[40] L.F.M. da Silva, P.J.C. das Neves, R.D. Adams, A. Wang, J.K. Spelt, Analytical models of adhesively bonded joints - Part II: Comparative study, Int. J. Adhes. Adhes. 29 (2009) 331–341.
[41] A. Doitrand, D. Leguillon, Comparison between 2D and 3D applications of the coupled criterion to crack initiation prediction in scarf adhesive joints, Int. J. Adhes. Adhes. 85 (2018) 69–76.
[42] J. Hetherington, H. Askes, A mass matrix formulation for cohesive surface elements, Theor. Appl. Fract. Mech. 69 (2014) 110–117.
[43] R. Jairaja, G. Narayana Naik, Numerical studies on weak bond effects in single and dual adhesive bonded single lap joint between CFRP and aluminium, Mater. Today: Proc. 21 (2020) 1064–1068.
[44] M.R. Khosravani, D. Anders, K. Weinberg, Influence of strain rate on fracture behavior of sandwich composite T-joints, Eur. J. Mech. A 78 (2019) 103821.
[45] L. Sun, C. Li, Y. Tie, Y. Hou, Y. Duan, Experimental and numerical investigations of adhesively bonded CFRP single-lap joints subjected to tensile loads, Int. J. Adhes. Adhes. 95 (2019) 102402.
[46] H. Hosseini-Toudeshky, F. Sheibanian, H.R. Oveysi, M.S. Goodarzi, Prediction of interlaminar fatigue damages in adhesively bonded jointsusing mixed-mode strain based cohesive zone modeling, Theor. Appl. Fract. Mech. 106 (2020) 102480.
[47] P. Davies, L. Soheir, J.Y. Cognard, A. Bourmaud, D. Choqueuse, E. Rinneert, R. CréacHcaded, Influence of adhesive bond line thickness on joint strength, Int. J. Adhes. Adhes. 29 (2009) 724–736.
[48] R. Kahraman, M. Sunar, B. Yilbas, Influence of adhesive thickness and filler content on themechanical performance of aluminum single-lap jointsbonded with aluminum powder filled epoxy adhesive, J. Mater. Process. Technol. 205 (2008) 183–189.
[49] D. Castagnetti, A. Spaggiari, E. Dragoni, Effect of bondline thickness on the static strength of structural adhesives under nearly-homogeneous shear stresses, J. Adhes. 87 (2011) 780–803.
[50] M.D. Banea, L.F.M. da silva, R.D.S. Campilho, The effect of adhesive thickness on the mechanical behavior of a structural polyurethane adhesive, J. Adhes. 91 (2015) 331–346.